ELSEVIER

Journal of Crystal Growth 204 (1999) 224–228

JOURNAL OF CRYSTAL GROWTH

www.elsevier.nl/locate/jcrysgro

A multiphase-field model: sharp interface asymptotics and numerical simulations of moving phase boundaries and multijunctions

Britta Nestler*

Foundry Institute, RWTH Aachen, Intzestrasse 5, D-52072 Aachen, Germany

Received 17 September 1998; accepted 3 March 1999
Communicated by J.B. Mullin

Abstract

In this paper we bring together, compare and extend two recent developments in a special formulation of an anisotropic multiphase-field model; namely the results of sharp interface asymptotic analysis by Nestler and Wheeler [B. Nestler, A.A. Wheeler, Phys. Rev. E 57 (3) (1998) 2602.] and numerical simulations of moving phase boundaries and multijunctions by Garcke et al. [H. Garcke, B. Nestler, B. Stoth, Physica D 115 (1998) 87; SIAM J. Appl. Math., in press]. First, we present the formulation of the multiphase-field model, which includes surface energy anisotropy. Then we state, how the leading order conditions at both interfaces and junctions can succinctly be derived in the sharp interface limit by introducing a generalized Cahn–Hoffman ξ-vector formalism and by using the motion of a stress tensor. These analytical results contain that the force balance at multijunctions is recovered, which comprises Young's law and, in the anisotropic case, additional shear forces. Next, we present numerical simulations of evolving phase boundaries and junctions, concentrating on the case of isotropic phases. We find that our numerical solutions of the multiphase-field model compare favorably with the exact solutions of the sharp interface analytical results. We observe that the classical angle conditions at trijunctions are obtained numerically. Finally, we perform simulations of grain growth evolution and numerically verify the validity of the qualitative features of the von Neumann law.

Keywords: Phase-field models; Sharp interface asymptotics; Numerical simulations; Triple junction dynamics; Multiphase diffusion

1. Introduction

The focus of this paper is the comparison of sharp interface asymptotic results with numerical simulations using a recent formulation of a multiphase-field model. In Section 2, we briefly define the multiphase-field model and show how the anisotropy of the surface energies between the different phases is included into this model. We summarize the main features of our work [1], in which the correct form of the Gibbs–Thomson–Herring equation at interfaces as well as the anisotropic force balance at multijunctions are recovered in the sharp interface limit using a generalized Cahn–Hoffman ξ-vector formalism. In related work [2], we used formal asymptotic analysis to determine

* Tel.: + 49-241-804067; fax: + 49-241-8888276.
E-mail address: britta@gi.rwth-aachen.de (B. Nestler)

0022-0248/99/$ - see front matter
PII: S0022-0248(99)00154-2

the asymptotic singular limit of a multiphase Allen–Cahn system. In Section 3, we present numerical simulations which were performed with the multiphase-field model described in the previous section. The numerical results of the interfaces and junctions compare very well with our analysis. A more precise discussion of the numerical calculations is described in Ref. [3].

2. The model and results of the sharp interface limit

We consider a system of N bulk phases which are, in the model, represented by N phase-field variables ϕ_α, $\alpha = 1, \ldots, N$. The dimensionless anisotropic free energy functional associated with this system is given by

$$\begin{aligned}\mathcal{F} &= \int_V \mathcal{L}(\boldsymbol{\phi}, \nabla\boldsymbol{\phi})\,\mathrm{d}V \\ &= \int_V \sum_{\beta=1}^{N}\sum_{\alpha=1}^{\beta}\left[36\varepsilon_{\alpha\beta}\gamma_{\alpha\beta}^2(\boldsymbol{r}_{\alpha\beta}) + \frac{1}{4\varepsilon_{\alpha\beta}}g_{\alpha\beta}(\boldsymbol{\phi})\right] \\ &\quad + \sum_{\alpha=1}^{N} h_\alpha(\boldsymbol{\phi}, T)\,\mathrm{d}V, \qquad (1)\end{aligned}$$

where $\mathcal{L}$ is the Lagrangian density, $\varepsilon_{\alpha\beta}$ is proportional to the barrier heights of the intercorrelation bulk potentials $g_{\alpha\beta}(\boldsymbol{\phi})$. The terms $h_\alpha(\boldsymbol{\phi}, T)$ represent the free energy density of bulk phases and determine deviation from thermodynamical equilibrium. Anisotropy of the surface energies is realized by assuming the parameters $\gamma_{\alpha\beta}$ to depend on $\boldsymbol{r}_{\alpha\beta} = \phi_\alpha\nabla\phi_\beta - \phi_\beta\nabla\phi_\alpha$. The governing equations for the phase fields describe the rate of each phase change in the system. Ensuring that the total free energy $\mathcal{F}$ decreases monotonically in time, these evolution equations can be derived from the gradient flow of $\mathcal{F}$

$$\frac{\partial\phi_\mu}{\partial t} = -M\frac{\delta\mathcal{F}}{\delta\phi_\mu} = M\left\{\boldsymbol{\nabla}\left(\frac{\partial\mathcal{L}}{\partial\nabla\phi_\mu}\right) - \frac{\partial\mathcal{L}}{\partial\phi_\mu}\right\},$$

$$\text{for } \mu = 1, \ldots, N,$$

where M represents a mobility that may generally be anisotropic and depend on orientation, $M = M(\boldsymbol{\nabla\phi})$. Using the explicit expression of $\mathcal{F}$ in Eq. (1) and the notion of generalized Cahn–Hoffman $\boldsymbol{\xi}$-vectors

$$\boldsymbol{\xi}_{\alpha\beta}(\boldsymbol{r}_{\alpha\beta}) = \frac{\partial\gamma_{\alpha\beta}(\boldsymbol{r}_{\alpha\beta})}{\partial\boldsymbol{r}_{\alpha\beta}} = \nabla_{r_{\alpha\beta}}\gamma_{\alpha\beta}(\boldsymbol{r}_{\alpha\beta}),$$

a straightforward calculation leads to the following rewritten form:

$$\begin{aligned}\frac{1}{M}\frac{\partial\phi_\mu}{\partial t} = \sum_{\alpha\neq\mu}^{N}\Bigg[&72\varepsilon_{\alpha\mu}[\boldsymbol{\nabla}\cdot(\gamma_{\alpha\mu}\boldsymbol{\xi}_{\alpha\mu}\phi_\alpha) + \gamma_{\alpha\mu}\boldsymbol{\xi}_{\alpha\mu}\cdot\boldsymbol{\nabla}\phi_\alpha] \\ &- \frac{1}{4\varepsilon_{\alpha\mu}}\frac{\partial g_{\alpha\mu}}{\partial\phi_\mu}\Bigg] - \frac{\partial h_\mu}{\partial\phi_\mu} - \lambda. \qquad (2)\end{aligned}$$

The Lagrange multiplier λ accounts for the constraint that all components ϕ_α sum up to one. Furthermore, the introduction of $\boldsymbol{\xi}$-vectors provides an elegant and concise derivation of a sharp interface model in the asymptotic limit of $\varepsilon_{\alpha\beta} \to 0$. In this limit, the dimensionless form of the Gibbs–Thomson–Herring equation is obtained at all interfaces, see Refs. [1,2]. To investigate the leading order force balance at multijunctions, where $m\,(\leqslant N)$ bulk phases meet, we formulate a divergence-free stress tensor Ξ

$$\Xi = \sum_{\mu=1}^{N}\nabla\phi_\mu\otimes\frac{\partial\mathcal{L}}{\partial\nabla\phi_\mu} - \mathcal{L}I \text{ with } \nabla\cdot\Xi = 0.$$

Applying this definition to the multiphase-field model above, using the divergence theorem, taking the sharp interface limit and evaluating the Lagrangian density to leading order, the force balance at a multijunction follows to be

$$\sum_{\mu=0}^{m-1}\boldsymbol{F}_\mu = \boldsymbol{l}\times\sum_{\mu=0}^{m-1}\boldsymbol{\xi}_{\mu\mu+1} = 0, \qquad (3)$$

where $\boldsymbol{F}_\mu$ is the total force acting tangentially on the $\mu/\mu+1$ interface. The vector $\boldsymbol{l}$ is a unit vector that lies parallel to the multijunction. If we rewrite the last expression in spherical polar coordinates, the equation can be identified as Young's law plus additional shear forces due to surface energy anisotropy.

3. Numerical simulations

To solve the phase-field equations, Eq. (2), we have employed a finite difference discretization on a uniform rectangular mesh, an explicit algorithm for the time update and Neumann boundary

conditions. For more details about the numerical setup see Ref. [3]. In a series of simulations we have tested different choices of bulk free energies $g_{\alpha\beta}(\boldsymbol{\phi})$ in order to find the best calibration between numerical and physical parameters. Since, in these experiments, a higher order variant of the double obstacle potential, which we call $g(\boldsymbol{\phi})$, has proved to have the best properties, we choose the potential

$$g(\boldsymbol{\phi}) = \sum_{\alpha,\beta} g_{\alpha\beta}(\boldsymbol{\phi}) + \sum_{\alpha,\beta,\mu} g_{\alpha\beta\mu}(\boldsymbol{\phi})$$

$$= \sum_{\alpha,\beta} \phi_\alpha \phi_\beta + \sum_{\alpha,\beta,\mu} \delta_{\alpha\beta\mu} \phi_\alpha \phi_\beta \phi_\mu$$

for our simulations. The parameter $\delta_{\alpha\beta\mu}$ is chosen in such a way that the minimal curves, connecting two minima in the Gibbs simplex, lie along the edges of the Gibbs simplex. This ensures that no contribution of the third phase appears at a two phase boundary and during a phase transition of two phases. To treat the double obstacle potential numerically, we first solve the smooth part of the differential equation and then project back onto the Gibbs simplex. In the simulation results, a special grey shade is associated to each of the phases in the system. In Fig. 1a–Fig. 1f, we study the behavior and motion of trijunctions of three isotropic phases labeled 1, 2 and 3 (see Fig. 1b). As initial configuration, we always used a T-shape and set two of the three surface energies equal, $\gamma_{12} = \gamma_{13}$ and the other one different $\gamma_{23} \neq \gamma_{12}$. We display a series of trijunction calculations in which the ratio between two of the surface energies, $R = \gamma_{23}/\gamma_{12}$ is varied (Fig. 1b–Fig. 1f). We observe that the trijunction adjusts very rapidly with an angle condition that agrees, in all the cases described in Fig. 1, very well with the predictions from Young's law, Eq. (3). Subsequently, the curvature of the interface changes approaching a constantly transported profile and the motion is only driven by curvature (Fig. 1a).

Finally, we consider the process of grain ripening and grain growth in a system of four phases and of many grains. In Fig. 2a–Fig. 2c, we show the time evolution of three simulations with the same initial grain configuration, but with different choices of surface energies. In the system where all the surface energies are equal, all trijunctions have a 120° angle condition. In this case, characteristic features of the von Neumann law can be observed. In application to grain growth, the von Neumann law says that

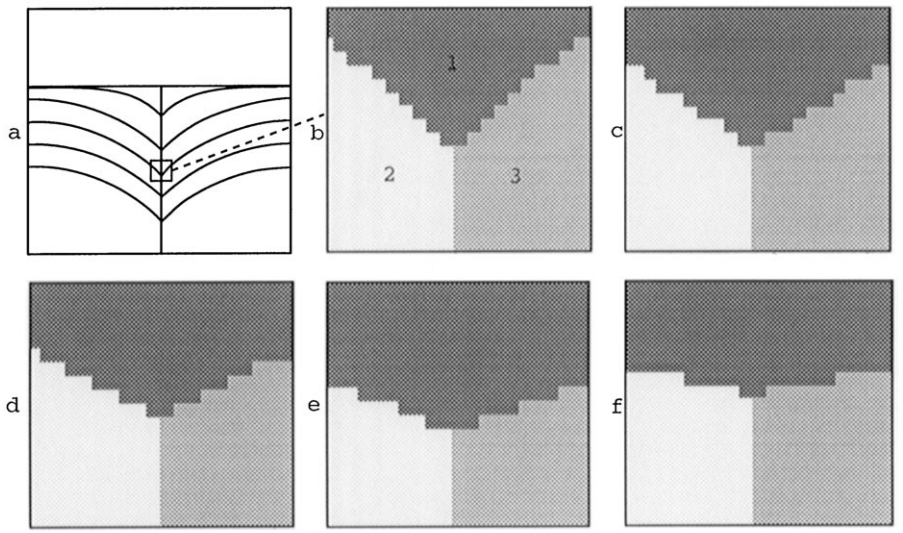

Fig. 1. Results of numerical calculations with surface energy ratios of $R = \gamma_{23}/\gamma_{12} = 1.532$, 1.286, 1.000, 0.684 and 0.347. These ratios correspond to triplejunction angles: $(\theta_1, \theta_2, \theta_3) = (80°, 140°, 140°)$, $(100°, 130°, 130°)$, $(120°, 120°, 120°)$, $(140°, 110°, 110°)$ and $(160°, 100°, 100°)$. The snapshots b–f show the triplejunction region in a high magnification.

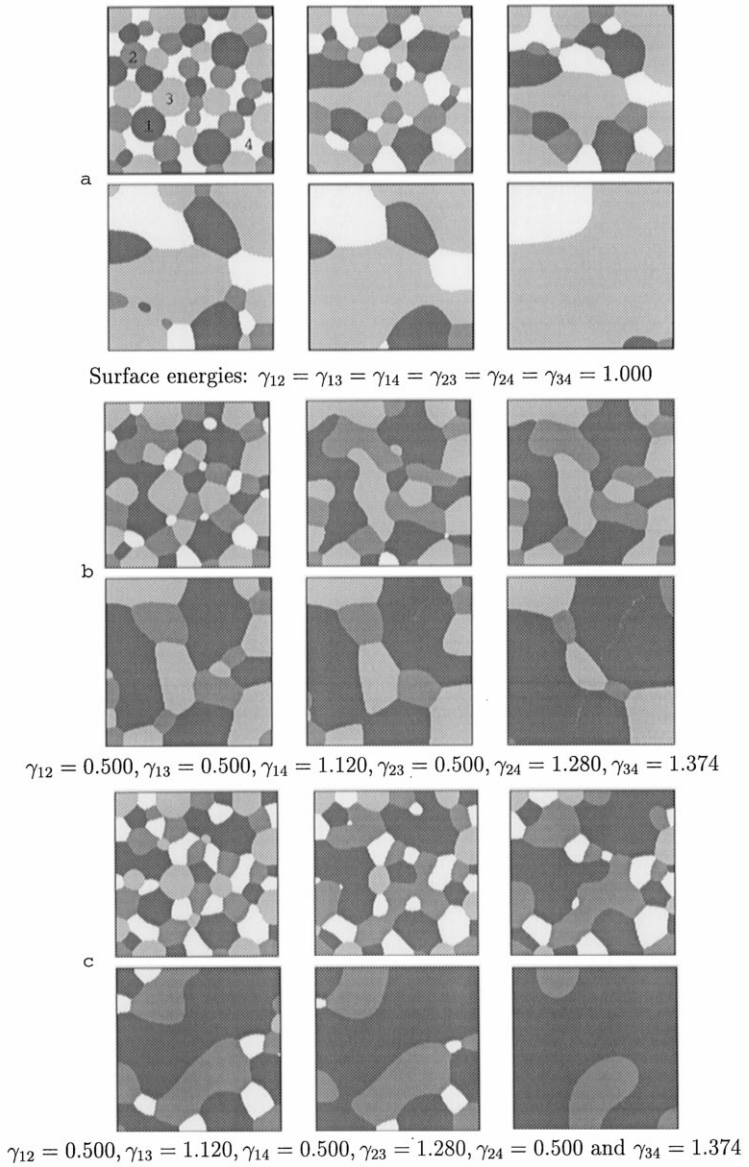

Fig. 2. Simulations of grain ripening with different sets of surface energies. For the three experiments, the snapshots are taken at the same time steps: $t = 0.00225$, 0.00675, 0.01125, 0.02250, 0.03375 and 0.06750.

grains with less than six neighbors shrink, grains with more than six neighbors grow and six-sided grains keep their area in time. From the choice of parameters, it can be seen that the values of the surface energies for the second and the third experiment (Fig. 2b and Fig. 2c) remain the same except that the ordering has changed. Furthermore, one of the possible four trijunctions in the system is forced to have a 120° angle condition, namely the 123-junction and the 124-junction in the second and the third simulation, respectively. We find that the phase that does not take part in the 120° trijunction disappears a long time before any other phase in the system.

Acknowledgements

The author gratefully thanks H. Garcke, B. Stoth and A.A. Wheeler for the joint work and excellent cooperation. This work was performed with support from the German Research Foundation (DFG) under grant number SA 335/25-2.

References

[1] B. Nestler, A.A. Wheeler, Phys. Rev. E 57 (3) (1998) 2602.
[2] H. Garcke, B. Nestler, B. Stoth, Physica D 115 (1998) 87.
[3] H. Garcke, B. Nestler, B. Stoth, SIAM J. Appl. Math., in press.